Published OnlineFirst July 27, 2017; DOI: 10.1158/1078-0432.CCR-17-1232

Cancer Therapy: Preclinical

Clinical Cancer Research

Association of FGFR1 with ERα Maintains Ligand-Independent ER Transcription and Mediates Resistance to Estrogen Deprivation in ER$^+$ Breast Cancer

Luigi Formisano[1,2], Kimberly M. Stauffer[3], Christian D. Young[1], Neil E. Bhola[1], Angel L. Guerrero-Zotano[1], Valerie M. Jansen[1], Mónica M. Estrada[4], Katherine E. Hutchinson[1], Jennifer M. Giltnane[3], Luis J. Schwarz[1], Yao Lu[1], Justin M. Balko[1,4,5], Olivier Deas[6], Stefano Cairo[6,7], Jean-Gabriel Judde[6], Ingrid A. Mayer[1,4], Melinda Sanders[3,4], Teresa C. Dugger[1], Roberto Bianco[2], Thomas Stricker[3,4], and Carlos L. Arteaga[1,4,5]

Abstract

Purpose: *FGFR1* amplification occurs in approximately 15% of estrogen receptor–positive (ER$^+$) human breast cancers. We investigated mechanisms by which *FGFR1* amplification confers antiestrogen resistance to ER$^+$ breast cancer.

Experimental Design: ER$^+$ tumors from patients treated with letrozole before surgery were subjected to Ki67 IHC, FGFR1 FISH, and RNA sequencing (RNA-seq). ER$^+$/*FGFR1*–amplified breast cancer cells, and patient-derived xenografts (PDX) were treated with FGFR1 siRNA or the FGFR tyrosine kinase inhibitor lucitanib. Endpoints were cell/xenograft growth, FGFR1/ERα association by coimmunoprecipitation and proximity ligation, ER genomic activity by ChIP sequencing, and gene expression by RT-PCR.

Results: ER$^+$/*FGFR1*–amplified tumors in patients treated with letrozole maintained cell proliferation (Ki67). Estrogen deprivation increased total and nuclear FGFR1 and FGF ligands expression in ER$^+$/*FGFR1*–amplified primary tumors and breast cancer cells. In estrogen-free conditions, FGFR1 associated with ERα in tumor cell nuclei and regulated the transcription of ER-dependent genes. This association was inhibited by a kinase-dead FGFR1 mutant and by treatment with lucitanib. ChIP-seq analysis of estrogen-deprived ER$^+$/*FGFR1*–amplified cells showed binding of FGFR1 and ERα to DNA. Treatment with fulvestrant and/or lucitanib reduced FGFR1 and ERα binding to DNA. RNA-seq data from *FGFR1*-amplified patients' tumors treated with letrozole showed enrichment of estrogen response and E2F target genes. Finally, growth of ER$^+$/*FGFR1*–amplified cells and PDXs was more potently inhibited by fulvestrant and lucitanib combined than each drug alone.

Conclusions: These data suggest the ERα pathway remains active in estrogen-deprived ER$^+$/*FGFR1*–amplified breast cancers. Therefore, these tumors are endocrine resistant and should be candidates for treatment with combinations of ER and FGFR antagonists. *Clin Cancer Res; 23(20); 6138–50. ©2017 AACR.*

Introduction

Amplification of the chromosomal region 8p11-12, the genomic location of *FGFR1*, has been reported in breast, ovarian, bladder, lung and oral squamous cancers, and in rhabdomyosarcoma (1–7). *FGFR1* amplification occurs in approximately 10% of patients with estrogen receptor–positive (ER$^+$)/HER2$^-$ breast cancer, where it is associated with early relapse following adjuvant tamoxifen therapy and with poor survival (8). Blockade of FGFR1 signaling by pharmacologic or genetic approaches in human breast cancer cells harboring *FGFR1* amplification leads to decreased cell growth and survival, suggesting *FGFR1* gene amplification is a surrogate of cancer cell dependence on aberrant FGFR activity (8).

FGFRs belong to the family of receptor tyrosine kinases (RTK) that consist of an extracellular ligand-binding domain linked to an intracellular catalytic protein kinase core via a single-pass transmembrane domain (TMD; ref. 9). Binding of FGF ligands induces receptor dimerization, activation of the kinase domain, and phosphorylation of C-terminal tyrosines to which adaptor

[1]Department of Medicine, Vanderbilt University Medical Center, Nashville, Tennessee. [2]Department of Clinical Medicine, University of Naples Federico II, Naples, Italy. [3]Department of Pathology, Microbiology & Immunology, Vanderbilt University Medical Center, Nashville, Tennessee. [4]Breast Cancer Program, Vanderbilt-Ingram Cancer Center, Vanderbilt University Medical Center, Nashville, Tennessee. [5]Department of Cancer Biology, Vanderbilt University Medical Center, Nashville, Tennessee. [6]XenTech, Evry, France. [7]LTTA Center, Department of Morphology, Surgery and Experimental Medicine, University of Ferrara, Ferrara, Italy.

Note: Supplementary data for this article are available at Clinical Cancer Research Online (http://clincancerres.aacrjournals.org/).

Corrected online January 10, 2019.

Corresponding Authors: Carlos L. Arteaga, Vanderbilt University Medical Center, 2220 Pierce Avenue, 777 PRB, Nashville, TN 37232. Phone: 615-936-3524; Fax: 615-936-1790; E-mail: carlos.arteaga@vanderbilt.edu; and Thomas P. Stricker, thomas.stricker@vanderbilt.edu

doi: 10.1158/1078-0432.CCR-17-1232

Published OnlineFirst July 27, 2017; DOI: 10.1158/1078-0432.CCR-17-1232

Translational Relevance

ER$^+$/*FGFR1*–amplified breast cancer cells and tumors retain proliferation and ERα genomic activity despite estrogen deprivation therapy. Combined inhibition of ERα and FGFR1 induced regression of ER$^+$/*FGFR1*–amplified breast cancer cells and patient-derived xenografts, supporting further development of combinations of ER and FGFR antagonists for the treatment of patients with this subtype of breast cancer.

proteins dock, followed by activation of signal transduction pathways, including PI3K/AKT, RAS/RAF/MEK/ERK, phospholipase Cγ (PLCγ) and STATs (10). In addition, there is strong evidence that FGFRs traffic to the nucleus, where they may function in a different manner to classic transmembrane RTKs (11). For example, nuclear FGFR3 has been shown in the nucleus of malignant and nonmalignant breast epithelial cells (12). A nuclear interaction of FGFR2, STAT5, and progesterone receptor (PR), associated with PR/STAT5–regulated gene expression and breast cancer progression was also reported (13). Other studies have reported nuclear localization and a nucleus-specific function of FGFR1 in nonmammary cells (14–17). Medulloblastoma cells transfected with FGFR1-eGFP and evaluated by immunofluorescence (IF) have shown FGFR1 is associated with cell membranes, cytosol, and nuclear compartments (17). Substitution of the atypical TMD of FGFR1 (β-sheet containing polar amino acids) with the typical TMD of FGFR4 (α-helical, hydrophobic) prevents the nuclear localization of FGFR1 (18). Inability of both the full-length and cleaved forms of FGFR1 to localize to the nucleus results in reduced migration and invasiveness of cancer cells (15, 16). Finally, Chromatin immunoprecipitation sequencing (ChIP-seq) studies revealed that FGFR1 binds nuclear transcription factors involved in neural and muscle development (19).

Amplification of the *FGF3/4/19* ligand genes on chromosome 11q12-14 occurs in approximately 15% of human breast cancers (20, 21). Notably, one third of *FGFR1*-amplified tumors also harbor amplification of *CCND1*, *FGF3*, *FGF4*, and *FGF19* (22). This coamplification has also been associated with resistance to estrogen deprivation in ER$^+$ breast cancer and poor patient outcome (22), suggesting the possibility of ligand–receptor cooperativity.

Herein, we investigated mechanisms by which *FGFR1* amplification confers resistance to antiestrogens in ER$^+$ breast cancer. In a cohort of patients with ER$^+$ breast cancer treated with the aromatase inhibitor letrozole, we observed that tumors with *FGFR1* amplification maintained their proliferation despite drug-induced estrogen deprivation and exhibited nuclear localization of FGFR1. Estrogen deprivation also resulted in an increase of total and nuclear FGFR1 as well as FGF3/4/19 ligand expression in ER$^+$/*FGFR1*–amplified breast cancer cells. FGFR1 coupled with ERα to drive estrogen-independent transcription of ERα-responsive genes. The association of FGFR1 with ERα was inhibited upon transfection with a kinase-dead FGFR1 mutant and by pharmacologic inhibition of FGFR1. Finally, combined inhibition of FGFR1 and ERα with fulvestrant and lucitanib reduced the association of FGFR1 and ERα and growth of ER$^+$/*FGFR1*–amplified patient-derived xenografts (PDX). We propose a physical interaction between FGFR1 and ERα provides a mechanistic explanation for how *FGFR1* amplification contributes to resistance to endocrine therapy in ER$^+$ breast cancer.

Materials and Methods

Clinical trial and tumor biopsies

Tumor samples were obtained from patients with stage I–III operable ER$^+$/HER2$^-$ breast cancer enrolled in a clinical trial of the aromatase inhibitor letrozole administered for 2 weeks prior to surgery (NCT00651976; ref. 23). Patients provided written informed consent according to a protocol approved by the Vanderbilt-Ingram Cancer Center Institutional Review Board. Intraoperative biopsies or surgical specimens, snap-frozen in liquid nitrogen and formalin-fixed paraffin-embedded (FFPE), were obtained from each patient's tumor. IHC was conducted in both the pretreatment biopsy and in the posttreatment surgical biopsy of both tumors for Ki67 (Dako #M7240), ER (Santa Cruz Biotechnology #sc542) and PR (Dako #M3569). IHC for ER and PR was conducted according to methods reported elsewhere (24). FFPE tumor sections were scanned at ×100 magnification, and the area containing the highest number of positive cells was selected. Positive and negative tumor cells were manually counted at 400×; the percentage of positive cells was calculated with at least 1,000 viable cells. Ki67 IHC was scored by two independent pathologists (M.M. Estrada and J.M. Giltnane).

Cell lines

Cell lines were obtained from ATCC between 2014 and 2016 and maintained in DMEM/10% FBS (Gibco). Long-term estrogen-deprived (LTED) cells were generated upon long-term culture in phenol red-free IMEM/10% dextran charcoal–treated FBS [DCC-FBS; Hyclone, contains <0.0367 pmol/L 17β-estradiol (E2)] for 3 to 8 months until exponentially growing, hormone-independent cells emerged as described previously (25). Cell lines were authenticated by ATCC prior to purchase by the STR method. Cell lines were not authenticated after purchase. Mycoplasma testing was conducted for each cell line before use. All experiments were performed less than 2 months after thawing early passage cells.

FGFR1 and *CCND1* FISH

FGFR1 and *CCND1* copy number was measured by FISH analysis in FFPE tumor sections (see Supplementary Methods).

Cell proliferation

Cells were plated in 10% DCC-FBS ± FGF3 100 ng/mL or ± 2 μmol/L lucitanib for 7 or 14 days before being trypsinized and counted using a Coulter Counter (Beckman Coulter), or fixed and stained with crystal violet followed by quantification by spectrophotometric detection at 490 nm using a plate reader (GloMax-Multi Detection System, Promega; see Supplementary Methods).

Viral transduction

FGFR1 wild-type and GFP-expressing lentiviral constructs were generated in the pLX302 Gateway vector (Open Biosystems); FGFR1/TK− (K514M) pLX302 was created by site-directed mutagenesis by Genewiz. To generate stably transduced lines, 4 μg of the FGFR1, FGFR1/TK− (K514M), and GFP-pLX302 constructs was cotransfected with 3 μg psPAX2 (plasmid encoding gag, pol, rev, and Tat genes), and 1 μg pMD2G envelope plasmid (Sigma

Published OnlineFirst July 27, 2017; DOI: 10.1158/1078-0432.CCR-17-1232

Aldrich) into 293FT cells using Lipofectamine 2000 (Thermo Fisher Scientific). 293FT growth media were changed 24 hours posttransfection; virus-containing supernatants were harvested 48 and 72 hours posttransfection, passed through a 0.45-μm filter, diluted 1:4, and applied to target cells with 8 μg/mL polybrene (Sigma Aldrich). Virus-producing cells were selected in 1 μg/mL puromycin.

Proximity ligation assay

Proximity ligation assay (PLA) was performed in cultured cells and in FFPE primary tumor sections to detect FGFR1/ERα localization using the Duolink Detection Kit (#DUO92101, Sigma; see Supplementary Methods).

Gene expression analyses

CAMA1 cells were plated in estrogen-free media and treated ± 100 ng/mL FGF3/19 (Sigma) for 6 hours. Cells were harvested and RNA was purified using the RNeasy Kit (Qiagen). cDNA was generated using High-Capacity cDNA Reverse Transcription Kits (Applied Biosystems), followed by analysis of ERα pathway genes using the Estrogen Receptor PCR Array (Qiagen, PAHS-005Z). RNA sequencing (RNA-seq) data (see "RNA-seq and cDNA library construction" below) were aligned to human genome version 19 using the splice-aware aligner TopHat (v2.0.9), and isoform level expression was quantified using cufflinks. Expression levels were normalized across the data set using cuffnorm. We compared genes upregulated in *FGFR1*-amplified versus *FGFR1* nonamplified cancers ($\geq$2.0-fold, FDR-adjusted $P \leq 0.05$). These genes were entered into gene set enrichment analysis (GSEA) as a ranked list. Gene sets with an FDR of <0.01 were considered to be enriched in *FGFR1*-amplified versus nonamplified tumors (see Supplementary Methods).

ChIP/DNA sequencing

ChIP was done using CAMA1 cells plated in estrogen-free media ± 100 ng/mL FGF3 and treated with 2 μmol/L lucitanib, 1 μmol/L fulvestrant, or the combination. Cells were grown to 80% confluency, washed 3 times in ice-cold PBS, and then fixed for 10 minutes at room temperature using 7% formaldehyde, followed by quenching with 2.5 mol/L glycine. Cells were first lysed using Farnham lysis buffer and then with nuclei lysis buffer (50 mmol/L Tris-HCl pH 8.0, 10 mmol/L EDTA pH 8.0, 1% SDS). Chromatin was sonicated using a Covaris LE220 with the following conditions: 35 minutes at peak power 350, duty factor 15, 200 cycles/burst, and average power 52.5; 200 μL of the chromatin was saved for input. Sonicated chromatin was diluted using ChIP Dilution Buffer (50 mmol/L Tris-HCl pH 8.0, 0.167 mol/L NaCl, 1.1% Triton X-100, 0.11% sodium deoxycholate), RIPA-150, protease inhibitors, and sodium butyrate. ERα (sc-8002) and FGFR1 (ab10646) antibodies were linked to magnetic anti-mouse and anti-rabbit Dynabeads, respectively, and then incubated with chromatin for >12 hours at 4°C. Immunoprecipitates (IP) were washed with the following buffers (RIPA-150, RIPA-500, RIPA-LiCl, and TE Buffer) for 5 minutes each. Chromatin-IPs were eluted from the beads, treated with RNase A at 65°C with shaking for 4 hours to reverse crosslinks, followed by proteinase-K treatment at 55°C for 1 hour. Next, DNA was purified using phenol–chloroform extraction, followed by ethanol precipitation and subsequent quantification by Qubit. Standard Illumina ChIPseq Library Kits were used to build sequencing libraries. Libraries were sequenced at Vanderbilt Technologies for Advanced Genomics (VANTAGE) Core Resource as SR50 on a HiSeq3000. Each antibody pulldown and the corresponding matching input was sequenced. The resulting sequencing files were aligned to human genome version 19 by BWA (Burrows–Wheeler aligner). For each replicate, peaks were called comparing with matched input, using MACS14 and default settings. The intersection of peak calls from each replicate was used to define the peak call set for each condition. Peaks were assigned to closest genes using annotatePeaks.pl in the HOMER analysis suite, and heatmaps were generated using ngs.plot.

ChIP/quantitative PCR

ChIP was performed in CAMA1 cells as described above. DNA was analyzed by real-time qPCR in triplicate with Sso Advanced SYBR Green Supermix (Bio-Rad) in a CFX qPCR machine (Bio-Rad). The fold enrichment of ChIP samples was calculated using the $2^{\Delta C_t}$ (threshold cycle) method. C_t values for ERα-ChIP and FGFR1-ChIP samples were normalized to input DNA C_t values, and then independently to respective negative control C_t values to account for antibody background. Primer sequences are listed in Supplementary Table S1.

RNA-seq and cDNA library construction

Core biopsies were flash frozen in liquid N_2 and stored at −80°C until RNA extraction was performed as described elsewhere (26). Total RNA was quantified using the Quant-iT RiboGreen RNA Assay Kit (Invitrogen) and normalized to 4 ng/μL; 200 ng of each sample was used for library preparation in an automated variant of the Illumina Tru Seq RNA Sample Preparation protocol (Revision A, 2010). This method uses oligo(dT) beads to select mRNA from the total RNA sample and is followed by heat fragmentation and cDNA synthesis from the RNA template. The resultant cDNA went through library preparation (end repair, base "A" addition, adapter ligation, and enrichment) using Broad Institute–designed indexed adapters for multiplexing. After enrichment, libraries were quantitated with qPCR using the KAPA Library Quantification Kit for Illumina Sequencing Platforms and pooled equimolarly. The entire process was performed in a 96-well format with all pipetting done by either the Agilent Bravo or PerkinElmer JANUS Mini liquid handlers.

Nonstranded Illumina RNA-seq

Pooled libraries were normalized to 2 nmol/L and denatured using 0.2 N NaOH prior to sequencing. Flowcell cluster amplification and sequencing were performed according to the manufacturer's protocol using either the HiSeq 2000 v3 or HiSeq 2500. Each run was a 76-bp, paired-end run with an eight-base index barcode. Data were analyzed using the Broad Picard Pipeline, which includes demultiplexing and data aggregation. TopHat spliced aligner software was used to map sequencing reads and to generate a BAM file for each tumor (27). RNA-seq GCT files were generated from BAM files using RNA-SeQC (28).

Xenograft studies

These studies were approved and performed in accordance with the Vanderbilt Institutional Animal Care and Use Committee. We used two $ER^+/HER2^-$/*FGFR1*–amplified PDXs. PDX T272 (XenTech) required estrogen supplementation in the drinking water (8.5 mg/L estrogen) to grow as tumors in female athymic nude mice (Envigo). The second PDX, TM00368 (The Jackson Laboratory), was implanted in female ovariectomized SCID/beige

Published OnlineFirst July 27, 2017; DOI: 10.1158/1078-0432.CCR-17-1232

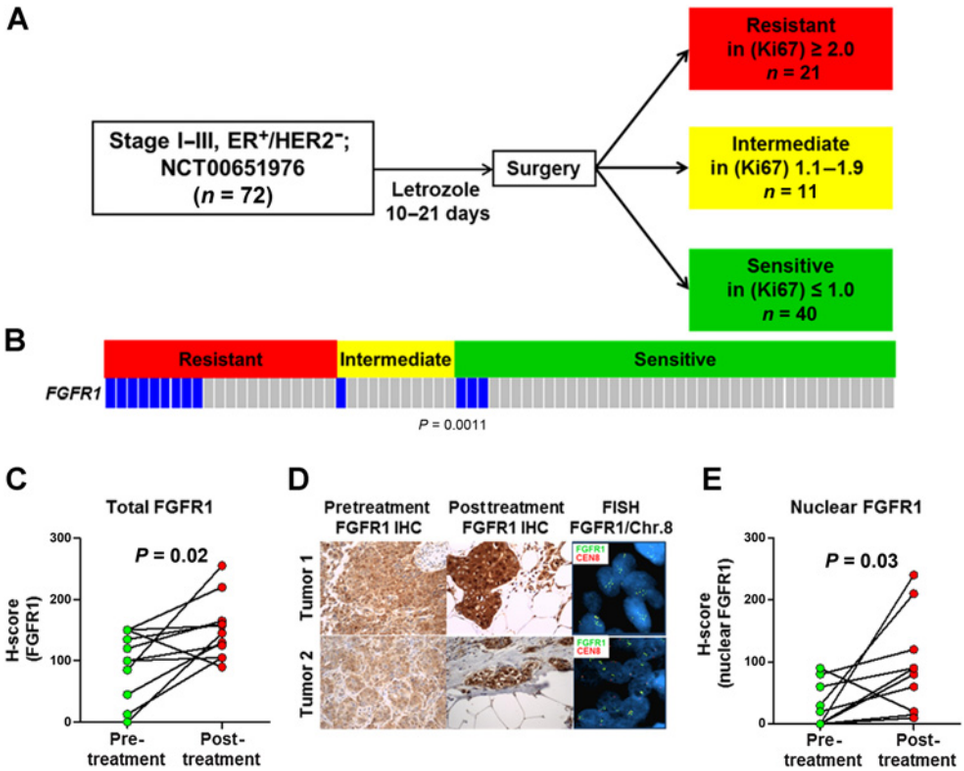

Figure 1.

FGFR1 amplification and overexpression associate with endocrine resistance in ER$^+$ breast cancer. **A,** Clinical trial schema: patients with stage I–III, ER$^+$/HER2$^-$ breast cancer were treated with letrozole for 10 to 21 days. Surgery was performed following treatment, and tumor response was categorized by calculating the natural log (ln) of the post-letrozole Ki67 score as determined by IHC analysis. **B,** *FGFR1* amplification, determined by FISH, was significantly associated with resistant versus intermediate or sensitive tumors ($P < 0.05$, Student t test). **C–E,** FFPE sections from *FGFR1*-amplified tumors were stained for FGFR1; the percent of FGFR1-positive tumor cells and staining intensity were assessed in both the cytoplasmic and nuclear compartments by a blinded expert breast pathologist (M.M. Estrada) to generate an H-score (**D**). The percent of cytoplasmic and nuclear FGFR1$^+$ tumor cells and their staining intensity were assessed by a blinded expert pathologist (M.M. Estrada) to generate an H-score. Total and nuclear FGFR1 H-scores are shown in **C** and **E,** respectively (Student t test). Both total and nuclear FGFR1 staining was higher in posttreatment tumor sections.

mice (The Jackson Laboratory) supplemented with a subcutaneous 21-day release, 0.25-mg 17β-estradiol pellet (Innovative Research of America). Tumors were serially transplanted in athymic or SCID/beige mice under general anesthesia. When xenografts reached a volume $\geq$200 mm^3, mice were randomized to treatment with vehicle, lucitanib (10 mg/kg/day orally for T272 or 7 mg/kg/day orally for TM00368), fulvestrant (5 mg/week s.c.) or both drugs ($n = 10$ per group for T272 and $n = 8$ per group for TM00368). Tumor diameters were measured using calipers twice a week, and volume in mm^3 calculated with the formula: volume = width^2 × length/2. When tumor volume exceeded 2 cm^3 or at the end of treatment, mice were sacrificed and tumors harvested 1 hours after the last dose of lucitanib. Portions of tumors were snap frozen or fixed in 10% neutral-buffered formalin and embedded in paraffin for subsequent analyses. Five-micron paraffinized sections were used for IHC using Y653/54 phosphorylated FGFR1 (Abcam #111124) and ERα (Santa Cruz Biotechnology #8002). Sections were scored by an expert pathologist (M.M. Estrada) blinded to treatment arm.

Statistical analysis

Results are representative of three independent experiments and are expressed as the mean ± SEM. A P value of less than 0.05, determined by Student t test, was considered statistically significant.

Results

FGFR1 amplification and overexpression is associated with endocrine resistance in ER$^+$ breast cancer

We studied 72 tumor biopsies from postmenopausal women with clinical stage I–III operable, ER$^+$/HER2$^-$ breast cancer treated with the aromatase inhibitor letrozole for 2 weeks prior to surgery (NCT00651976). Earlier studies have demonstrated that a Ki67 score 2 weeks after antiestrogen therapy can be utilized to predict which tumors are endocrine sensitive or resistant, as measured by their odds of recurrence following adjuvant endocrine therapy (29). We applied these metrics to our tumor set and categorized 40 tumors as sensitive [natural log (ln) of post-letrozole Ki67 $\leq$1.0 or $\leq$2.4% tumor cells], 11 tumors as intermediate responders (ln = 1.1–1.9 or 2.5%–7.3% tumor cells), and 21 tumors as resistant (ln $\geq$ 2.0 or $\geq$7.4% tumor cells; Fig. 1A). *FGFR1* copy number was determined in tumor sections by FISH. We observed *FGFR1* amplification in 9 of 21 (43%) resistant tumors compared with 3 of 40 (7%) sensitive tumors and 1 of 11 (10%) intermediate tumors (resistant vs. intermediate and sensitive tumors; P =

Published OnlineFirst July 27, 2017; DOI: 10.1158/1078-0432.CCR-17-1232

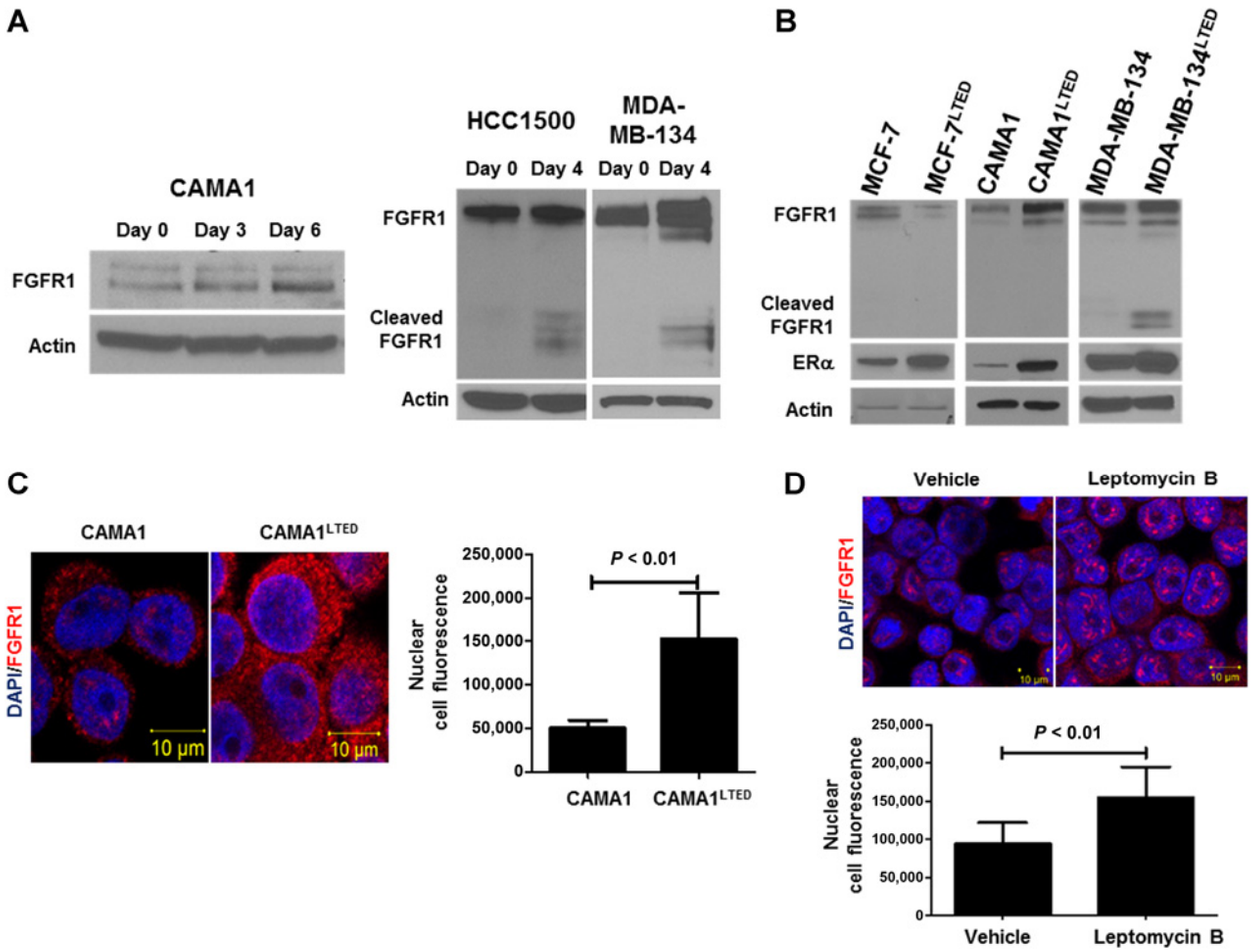

Figure 2.

Estrogen deprivation increases nuclear and cytosolic FGFR1 expression. **A,** Immunoblot analysis of lysates from CAMA1, HCC1500, and MDA-MB-134 cells exposed to short-term estrogen deprivation up to 6 days revealed an increase in FGFR1 expression over time. HCC1500 cells showed increased expression of the cleaved form of FGFR1. **B,** Immunoblot analysis of parental and LTED ER$^+$ cell lines following 24 hours of estrogen deprivation revealed an increase in FGFR1 and ERα in *FGFR1*-amplified CAMA1^{LTED} and MDA-MB-134^{LTED} cells but not in *FGFR1* nonamplified MCF-7 cells. **C,** Proximity ligation assay (PLA) to detect FGFR1 expression. Analysis of red, amplified loci by confocal microscopy confirmed immunoblot and FISH results in that CAMA1^{LTED} cells harbor more cytosolic and nuclear FGFR1 compared with CAMA1 parental cells. Each bar in the graph to the right of the PLA image represents the mean nuclear fluorescent signals ± SD of 3 wells. **D,** Immunofluorescence (IF) was performed in CAMA1 cells treated with vehicle or 30 ng/mL leptomycin B for 2 hours. Nuclear localization of FGFR1 was detected by confocal microscopy. Each bar represents the mean nuclear fluorescent signals ± SD of 3 wells.

0.0011; Fig. 1B). To correlate *FGFR1* copy number with protein levels, we performed IHC. FGFR1 protein levels correlated with gene amplification by FISH. In *FGFR1*-amplified cancers, we observed a significant increase in total and nuclear FGFR1 in posttreatment compared with pretreatment biopsies ($P < 0.05$; Fig. 1C and E). A letrozole-induced increase in both total and nuclear FGFR1 was not observed in tumors without *FGFR1* amplification (Supplementary Fig. S1A). There was no statistical correlation between *FGFR1* amplification and histologic tumor grade in the letrozole-resistant group (Supplementary Table S2).

Estrogen deprivation increases nuclear and cytosolic FGFR1 expression

To examine whether this same modulation of FGFR1 levels occurred in more controlled experimental conditions, we tested five ER$^+$/HER2$^-$ human breast cancer cell lines with and without *FGFR1* gene amplification as determined by FISH: CAMA1, MDA-MB-134, and HCC1500 cells are *FGFR1* amplified, while MCF-7 and ZR75.1 cells are not (Supplementary Fig. S2A). *FGFR1* amplification correlated with FGFR1 protein levels; MDA-MB-134 and HCC1500 cells express both full-length and cleaved FGFR1, while only full-length FGFR1 was detected in CAMA1 cells (Supplementary Fig. S2B). To mirror the acute estrogen deprivation induced by letrozole in primary tumors in the clinical trial (30), we cultured the *FGFR1*-amplified cell lines in estrogen-free medium for 4 to 6 days. Estrogen withdrawal resulted in an increase in FGFR1 expression in all *FGFR1*-amplified lines (Fig. 2A).

To determine whether long-term estradiol deprivation also affected FGFR1 expression, we generated three LTED cell lines as described previously (25): CAMA1^{LTED} and MDA-MB-134^{LTED} (*FGFR1*-amplified) and MCF-7^{LTED} (*FGFR1* nonamplified). As we had observed with acute estrogen deprivation, CAMA1^{LTED}

Published OnlineFirst July 27, 2017; DOI: 10.1158/1078-0432.CCR-17-1232

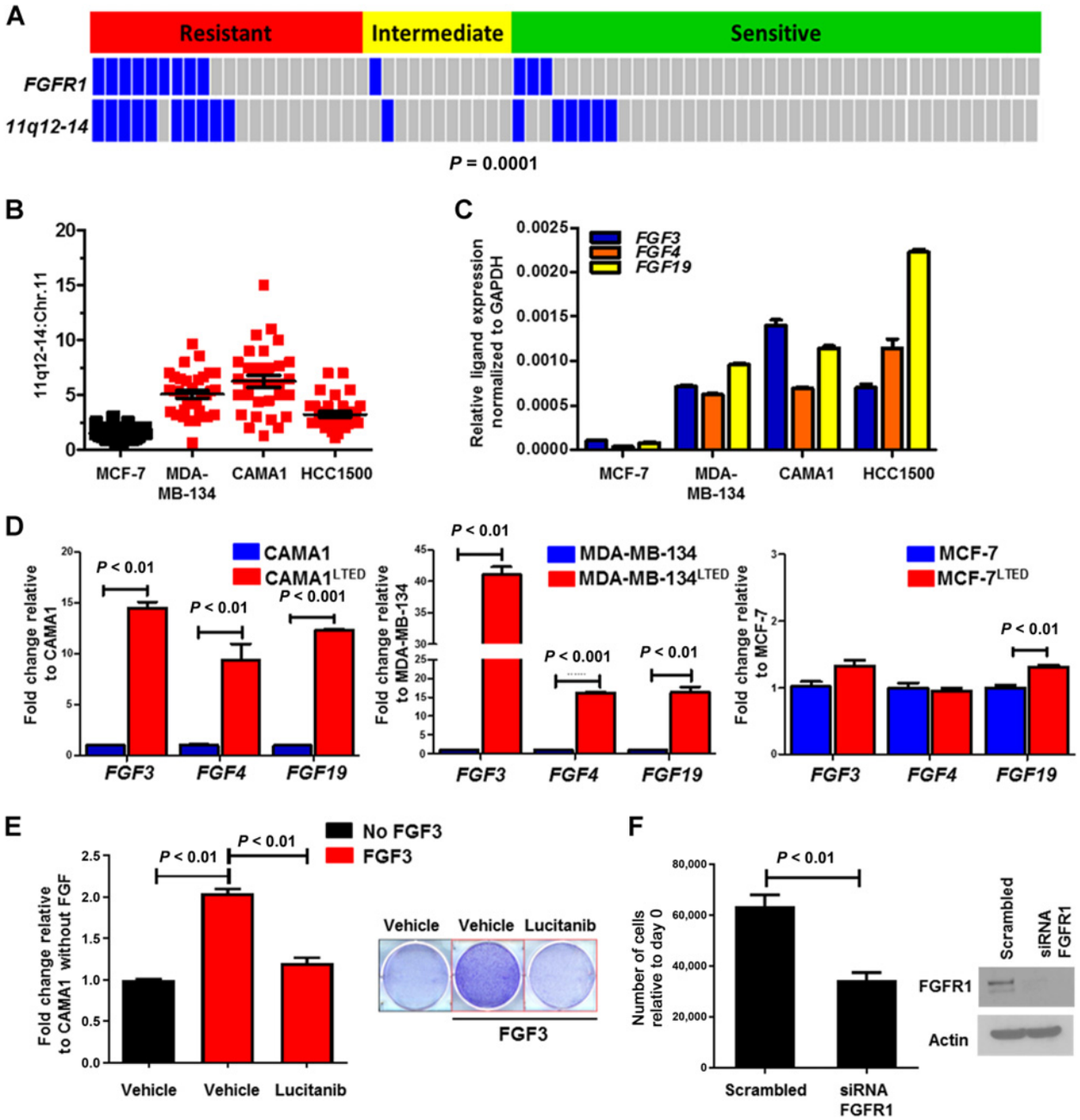

Figure 3.

FGF3/4/19 expression is upregulated upon estrogen deprivation. **A,** FISH analysis of primary tumor sections showed coamplification of *FGFR1* and *11q12-14* mainly in letrozole-resistant versus intermediate and sensitive cancers ($P = 0.0001$, Student *t* test). **B,** Coamplification of *11q12-14* was observed in ER$^+$/*FGFR1*-amplified cell lines MDA-MB-134, CAMA1, and HCC1500; the *y*-axis shows the 11q12-14:Chr.11 ratio. **C,** Relative transcript expression of FGF3/4/19 in the indicated cell lines was determined by qPCR as described in Materials and Methods. **D,** Transcript levels of FGF3/4/19 were higher in *FGFR1*-amplified LTED cells (CAMA1 and MDA-MB-134) but not in *FGFR1* nonamplified MCF-7^{LTED} cells compared with their parental counterparts (Student *t* test). **E,** CAMA1 cells were treated with 100 ng/mL FGF3 ± 2 μmol/L lucitanib in estrogen-free medium. After 15 days, plates were washed and stained with crystal violet, and their imaging intensity was quantified by spectrophotometric detection. Representative images and quantification of the integrated intensity values as % of vehicle-treated controls are shown (Student *t* test). **F,** CAMA1 cells were plated in 100-mm dishes and transfected with FGFR1 or control siRNAs as described in Materials and Methods. Medium containing 100 ng/mL FGF3 was replenished every 3 days. Seven days later, monolayers were harvested and cell counts determined using a Coulter Counter. Each bar in the left panel represents the mean cell number ± SD of triplicate wells (Student *t* test). FGFR1 knockdown was confirmed by immunoblot analysis of cell lysates from plates treated identically in parallel (right).

Published OnlineFirst July 27, 2017; DOI: 10.1158/1078-0432.CCR-17-1232

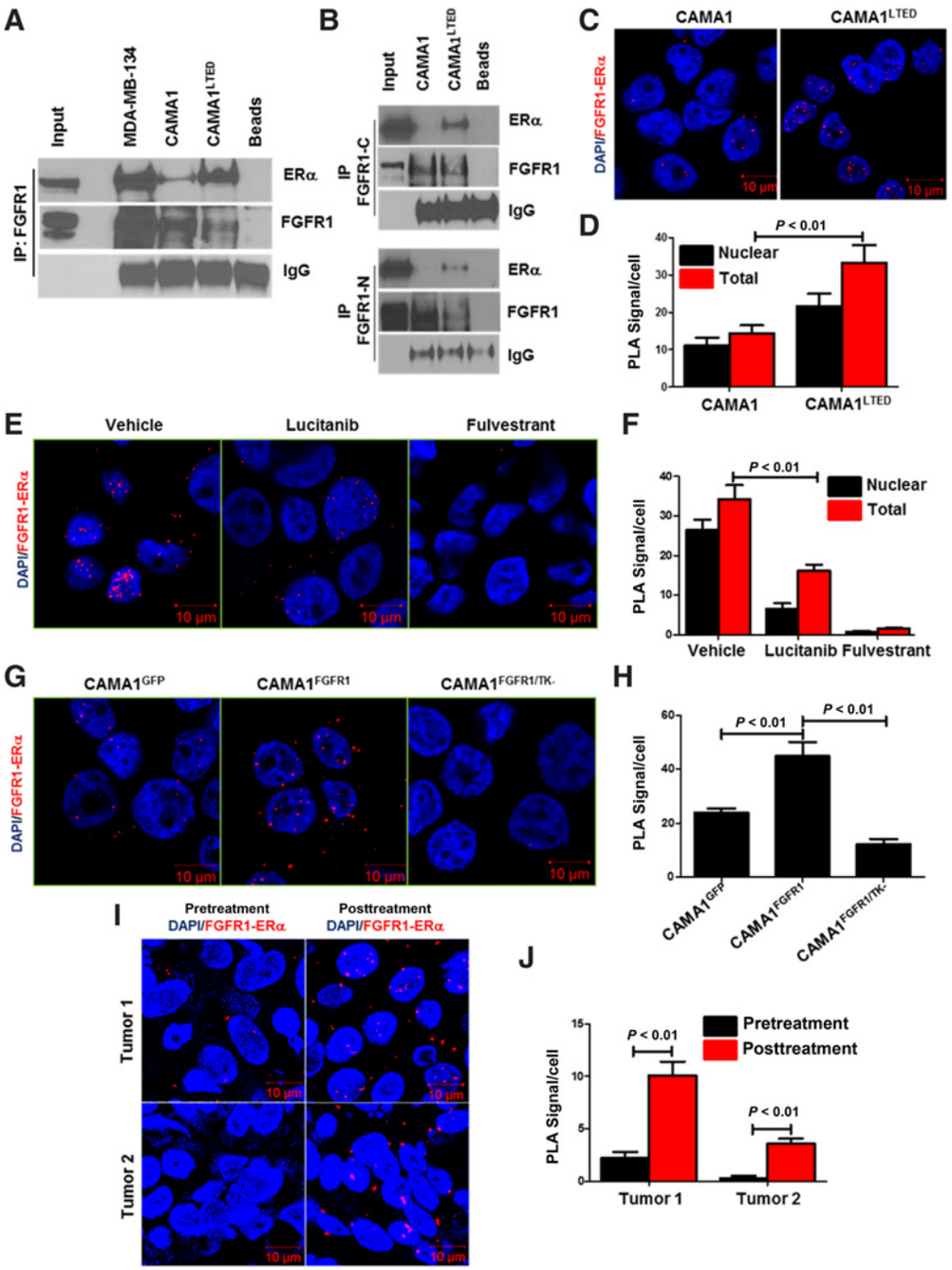

Figure 4.

Long-term estradiol deprivation increases the interaction of FGFR1 with ERα. **A,** FGFR1 was precipitated from MDA-MB-134, CAMA1 and CAMA1^{LTED} cell lysates; immune complexes were separated by SDS-PAGE and subjected to immunoblot analysis with an ERα antibody. CAMA1^{LTED} cells exhibited greater levels of FGFR1-ERα coimmunoprecipitation compared with CAMA1 cells. **B,** FGFR1 was precipitated from CAMA1 and CAMA1^{LTED} nuclear extracts with C-terminal (Abcam) and N-terminal (Cell Signaling Technology) FGFR1 antibodies; immune complexes were separated by SDS-PAGE and analyzed by ERα immunoblot. **C** and **D,** PLA of CAMA1^{LTED} cells showed greater nuclear colocalization of FGFR1 and ERα compared with parental CAMA1 cells. PLA foci/cell are quantified in **D**. **E** and **F,** CAMA1^{LTED} cells were treated with 2 μmol/L lucitanib or 1 μmol/L fulvestrant for 6 hours. Monolayers were subjected to PLA as described in Materials and Methods. Quantification of FGFR1–ERα complexes as PLA signals/cell is shown in **F**. Each bar represents the mean ± SD of 3 wells. **G** and **H,** CAMA1 cells were stably transfected with expression vectors encoding GFP, FGFR1, and FGFR1/TK– (K514M TK mutant), as described in Materials and Methods, and then plated in chamber slides followed by PLA. Quantification of FGFR1–ERα complexes as PLA signals/cell is shown in **H**. Each bar represents the mean ± SD of 3 wells. **I** and **J,** Paired pre- and post-letrozole primary tumor sections were subjected to PLA as described in Materials and Methods. Post-letrozole tumor cells exhibited more FGFR1–ERα complexes compared with pretreatment tumor cells as quantitated in **J**. Each bar represents the mean PLA signals/cell ± SD of 20 cells counted in each of 4 high-power fields.

Published OnlineFirst July 27, 2017; DOI: 10.1158/1078-0432.CCR-17-1232

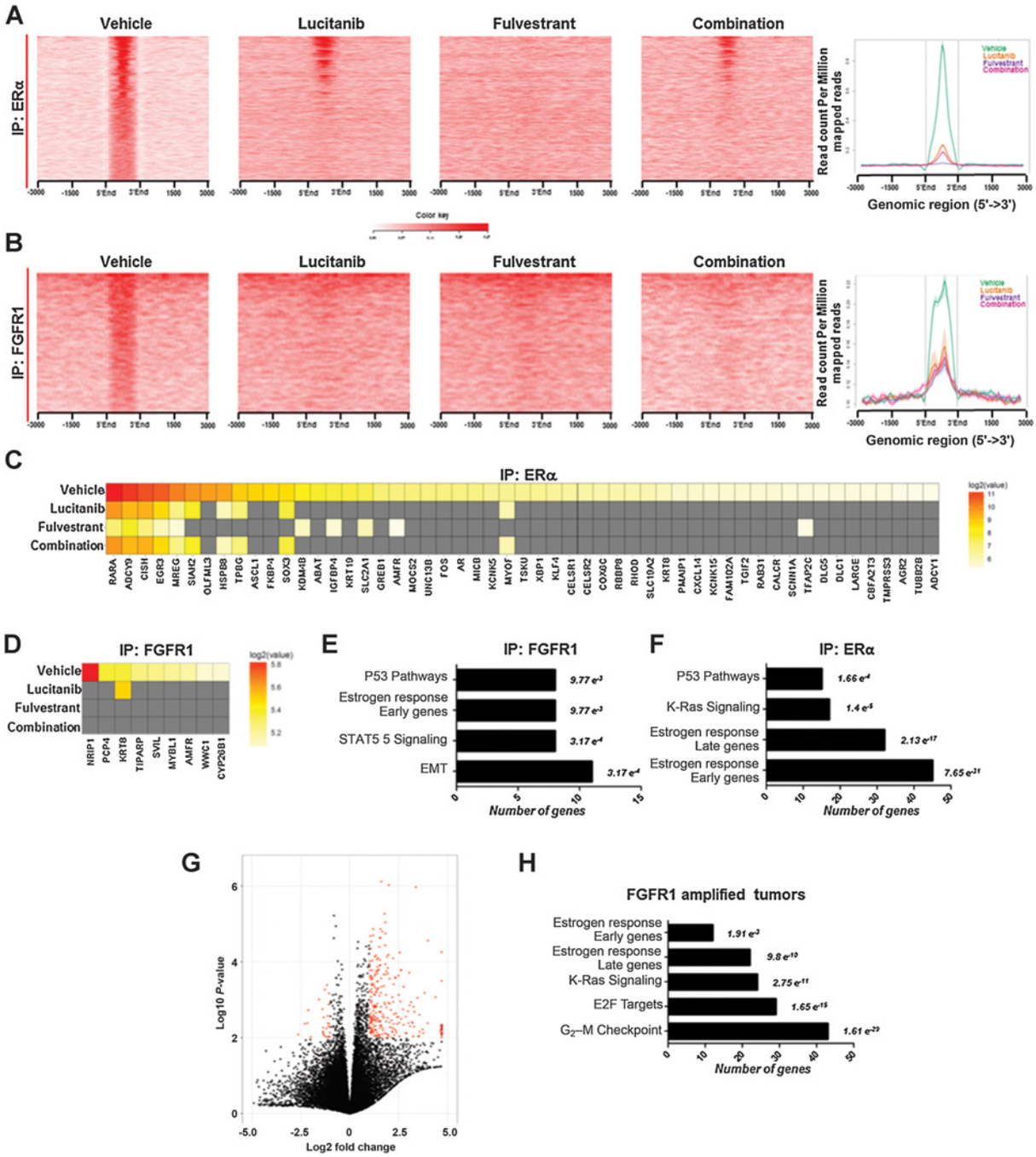

Figure 5.

Identification of FGF-sensitive ERα and FGFR1 genomic binding sites. **A** and **B,** CAMA1 cells were plated in estrogen-free medium and stimulated with 100 ng/mL FGF3 for 6 hours in the presence of 1 μmol/L fulvestrant, 2 μmol/L lucitanib, or the combination. Cells were harvested and subjected to ChIP-seq as described in Materials and Methods. Shown are heatmaps generated from ChIP-seq analysis of ERα (**A**) and FGFR1 (**B**) DNA binding. Treatment with fulvestrant, lucitanib, or the combination reduced binding of ERα (**A**) or FGFR1 (**B**) binding to DNA. Heatmaps represent the mean of two different experiments. **C** and **D,** Heatmaps of ChIP-seq data showing the effects of fulvestrant, lucitanib, or the combination on DNA/ERα-associated (**C**) and DNA/FGFR1-associated (**D**) genes, respectively, as shown in **A** and **B**. **E** and **F,** Gene set enrichment analysis (GSEA) of FGFR1- and ERα-associated genes. Numbers to the right of each bar represent the FDR q-value. **G,** Volcano plot analysis of differentially expressed genes in tumors from patients treated with letrozole in the clinical trial. Each data point represents the ratio of the average expression for a particular gene in *FGFR1*-amplified tumors ($n = 7$) versus *FGFR1* nonamplified tumors ($n = 25$). The red dots in the Volcano plot represent genes that are significantly up- or downregulated >2-fold with $P < 0.01$. **H,** GSEA of significantly enriched genes in *FGFR1*-amplified relative to *FGFR1* nonamplified tumors showed that ERα-related pathways are still active in estrogen-deprived (by letrozole treatment) ER^+/*FGFR1*-amplified primary tumors (**G**). Numbers to the right of each bar represent the FDR q-value.

Published OnlineFirst July 27, 2017; DOI: 10.1158/1078-0432.CCR-17-1232

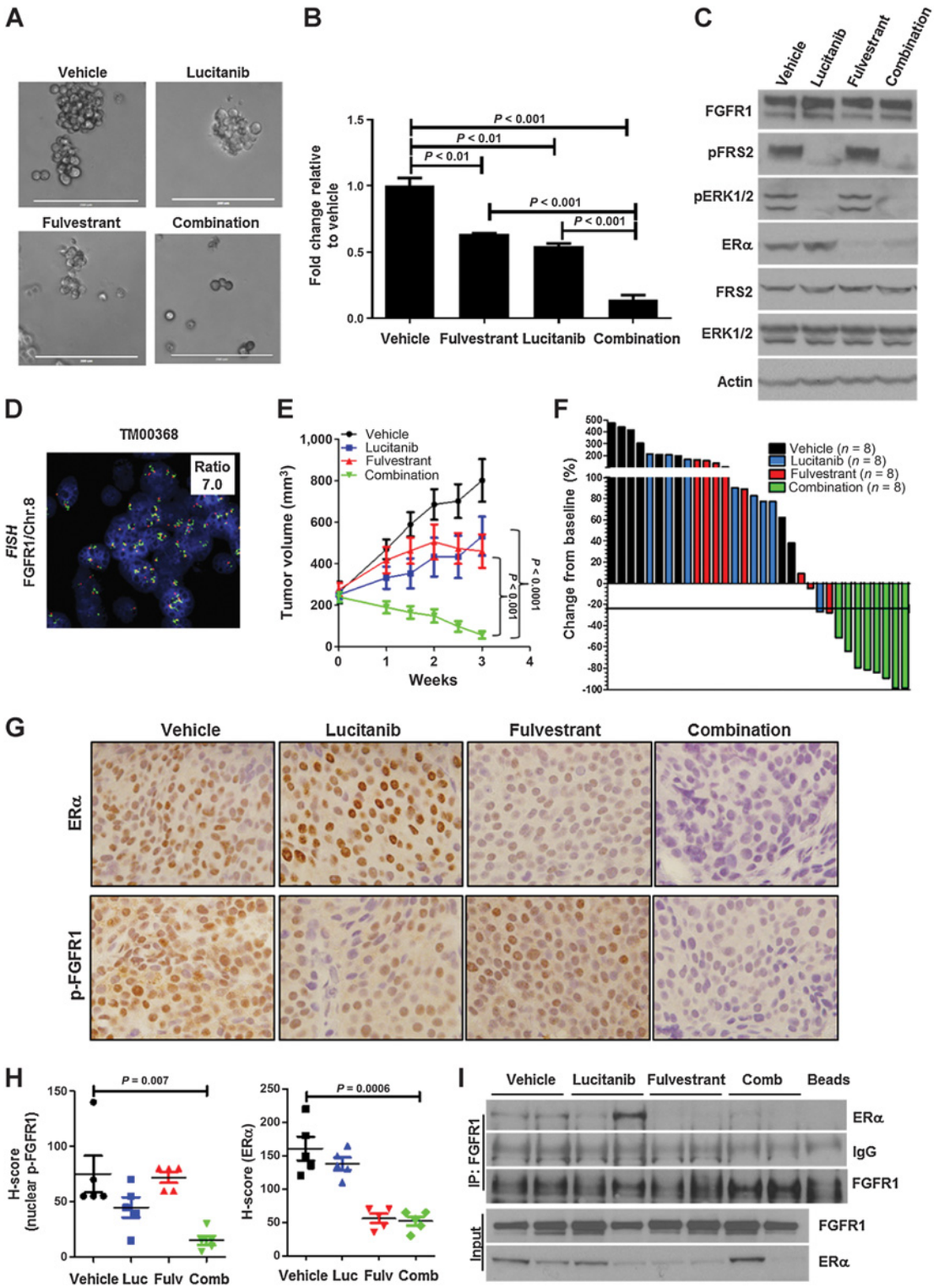

Figure 6.

Combined blockade of FGFR1 and ERα potently inhibits growth of ER$^+$/*FGFR1*-amplified breast cancers. **A** and **B,** CAMA1 cells were cultured in 3D Matrigel as described in Materials and Methods and treated with vehicle, 2 μmol/L lucitanib, 1 μmol/L fulvestrant, or the combination. After 15 days, images were captured from three different fields using a CK40 microscope. Quantitation of representative images is shown in **B**. Each bar represents the fold change in colony number relative to vehicle ± SD of three replicate wells repeated twice (Student *t* test). (*Continued on the following page.*)

Published OnlineFirst July 27, 2017; DOI: 10.1158/1078-0432.CCR-17-1232

and MDA-MB-134^{LTED} cells exhibited increased expression of full-length and cleaved FGFR1, respectively, whereas MCF-7^{LTED} cells showed a reduction in FGFR1 expression compared with parental MCF-7 cells. The LTED lines also displayed an increase in ERα levels compared with their parental counterparts (Fig. 2B). IF by confocal microscopy highlighted the increase in total and nuclear FGFR1 in CAMA1^{LTED} versus parental cells (Fig. 2C). We next treated CAMA1 cells with nuclear export inhibitor leptomycin B (31); this resulted in an increase in nuclear FGFR1 as measured by IF (Fig. 2D). Knockdown of *FGFR1* with siRNA confirmed the specificity of the FGFR1 antibody used for both immunoblot and IF analyses (Supplementary Fig. S2C and S2D).

FGF3/4/19 expression is upregulated upon estrogen deprivation

Approximately 30% to 40% of *FGFR1*-amplified breast cancers exhibit amplification of *CCND1*, *FGF3*, *FGF4*, and *FGF19* in chromosome 11q12-14 (32). Coamplification of these genes has been associated with reduced patient survival (22). By interrogating The Cancer Genome Atlas, we found that among the 13% of breast cancers with *FGFR1* amplification, 36% of these tumors also harbor *11q-12-14* amplification (Supplementary Fig. S3A and S3B; refs. 33, 34). Outcomes analysis of Kaplan–Meier plotter (breast cancer) showed that patients with coamplification of *FGFR1* and *CCND1/FGF3/FGF4/FGF19* treated with antiestrogen therapy exhibit a shorter time to relapse compared with patients without coamplified tumors (HR = 1.75; Supplementary Fig. S3C; ref. 35). Thus, we next investigated coamplification of *FGFR1* and *11q12-14* in our cohort of patients treated with letrozole. In this study, 8 of 9 (90%) *FGFR1*-amplified tumors exhibited coamplification of *FGF3/4/19*, and this coamplification strongly correlated with resistance to estrogen deprivation with letrozole (P = 0.0001; Fig. 3A). These data suggest that coamplification of *11q12-14* and *FGFR1* may play a causal role in endocrine resistance.

Notably, all *FGFR1*-amplified cell lines but not MCF-7 cells exhibited coamplification of *11q12-14* (Fig. 3B, Supplementary Fig. S4A). All *11q12-14*–amplified cell lines expressed markedly higher *FGF3/4/19* mRNA levels by qRT-PCR compared with MCF-7 cells (Fig. 3C). Similar to the effect on FGFR1 protein levels, 24 hours of estrogen deprivation increased *FGF3/4/19* mRNA expression 1.5- to 2-fold in all *FGFR1*-amplified cells (Supplementary Fig. S4B). This increase in *FGF3/4/19* was even more substantial in LTED *FGFR1*-amplified cells. In contrast, MCF7^{LTED} cells exhibited little or no increase in FGF ligands mRNA compared with MCF-7 parental cells (Fig. 3D).

These results also suggested that FGFs can provide a growth advantage to ER$^+$/*FGFR1*-amplified cells in estrogen-free conditions. To test this, we stimulated estrogen-starved CAMA1 cells with FGF3 in hormone-depleted media. Exogenous FGF3 enhanced estrogen-independent cell growth compared with unstimulated cells. Both treatment with the FGFR1 tyrosine kinase inhibitor (TKI), lucitanib (Fig. 3E; ref. 36), and transfection with FGFR1 siRNA prevented this outgrowth (Fig. 3F).

Long-term estradiol deprivation increases the interaction of FGFR1 with ERα

An association of FGFR1 with other nuclear proteins, such as ribosomal S6 kinase (RSK1) and CREB-binding protein (CBP), has been shown to be required for nuclear FGFR1 to induce gene expression in medulloblastoma and neuroblastoma cells (37). An interaction between FGFR1 and ERα has been reported to mediate lactotroph proliferation in the pituitary gland (38). Nuclear colocalization of PR, FGFR2, and STAT5 at DNA progesterone-responsive elements with increased transcription of PR/STAT5–regulated genes was also reported in human breast cancer cells (13). Thus, we next investigated whether ER and FGFR1 interacted in ER$^+$/*FGFR1*–amplified breast cancer cells. Antibody pulldown of FGFR1 from MDA-MB-134, CAMA1, and CAMA1^{LTED} whole-cell lysates coprecipitated ERα in all three cell lines (Fig. 4A). This association was stronger in MDA-134 and CAMA1^{LTED} cells compared with parental CAMA1 cells. We next confirmed the FGFR1–ERα association in CAMA1 and CAMA1^{LTED} nuclear extracts after precipitation with both C-terminal and N-terminal FGFR1 antibodies (Fig. 4B), suggesting with presence of full-length FGFR1 in cell nucleus. To quantitate this interaction, we performed PLAs. An interaction between FGFR1 and ERα was observed in the cytoplasm and nucleus of CAMA1 and CAMA1^{LTED} cells by PLA, particularly in the latter (Fig. 4C and D), in line with the immunoprecipitation experiments. Treatment with lucitanib reduced FGFR1/ERα complexes (Fig. 4E and F), suggesting this interaction requires FGFR1 tyrosine kinase (TK) activity.

To explore further whether the TK function of FGFR1 is required for FGFR1–ERα complex formation, CAMA1 cells were transduced with constructs expressing GFP, wild-type FGFR1, or a TK dead K514M FGFR1 mutant (FGFR1/TK$^-$). Overexpression of wild-type FGFR1 increased detectable FGFR1-ERα complexes, while overexpression of FGFR1/TK$^-$ decreased them as measured by PLA (Fig. 4G and H). Steady-state levels of pFRS2 were upregulated in cells transduced with wild-type FGFR1 but not with the FGFR1/TK$^-$ mutant (Supplementary Fig. S5A). Importantly, the CAMA1$^{FGFR1/TK-}$ cells were not able to grow in the absence of estradiol (Supplementary Fig. S5B and S5C). These data suggest that FGFR1 TK activity is important for estrogen-independent growth and the association of FGFR with ERα. Finally, we observed an increase of FGFR1-ERα complexes in post-letrozole compared with paired pre-letrozole FFPE tumor sections from 2 breast cancer patients harboring tumor coamplification of *FGFR1* and *11q12-14* (Fig. 4I and J).

FGF/FGFR pathway modulates ERα–DNA binding

To evaluate estrogen-independent genomic functions of ERα in ER$^+$/*FGFR1*–amplified cells, we performed ChIP followed by

(*Continued.*) **C,** CAMA1 cells were treated as in **A** and **B** for 6 hours, after which lysates were prepared and subjected to immunoblot analyses with the indicated antibodies. **E,** ER$^+$/HER2$^-$/*FGFR1*-amplified TM00368 PDXs were established in ovariectomized SCID/beige mice implanted with a subcutaneous 21-day release, 0.25-mg 17β-estradiol pellet. Once tumors reached ≥200 mm^3, mice were randomized to treatment with vehicle, fulvestrant (5 mg/kg/week), lucitanib (7 mg/kg/day), or both drugs for 3 weeks. Each data point represents the mean tumor volume in mm^3 ± SD (n = 8 per arm; ANOVA test). **F,** Bar graph showing the percent change in volume in individual TM00368 PDXs after 3 weeks of treatment relative to tumor volumes on day 0 (baseline). **G** and **H,** TM00368 tumors were harvested at the end of treatment. FFPE tumor sections were prepared and subjected to IHC with Y653/4 phosphorylated FGFR1 and ERα antibodies as described in Materials and Methods. The percent of phospho-FGFR1$^+$ and ER$^+$ tumor cells and their staining intensity was assessed by an expert breast pathologist (M.M. Estrada) blinded to the treatment to generate an H-score. Nuclear phospho-FGFR1 and ERα H-scores are shown (Student t test). **I,** FGFR1 was precipitated from lysates of TM00368 tumors harvested at the end of treatment; immune complexes were separated by SDS-PAGE and subjected to immunoblot analysis with the indicated antibodies. Bottom two lanes show FGFR1 and ERα content in lysates before intraperitoneal injection.

Published OnlineFirst July 27, 2017; DOI: 10.1158/1078-0432.CCR-17-1232

next-generation sequencing (ChIP-seq) in estrogen-deprived CAMA1 cells ± FGF3. First, we confirmed by cells fractionation that parental CAMA1 cells exhibited nuclear soluble and chromatin-bound FGFR1 at steady state (Supplementary Fig. S6A). Treatment with FGF3 shifted both ERα and FGFR1 to new binding sites that were unoccupied in the absence of the FGF ligand (Supplementary Fig. S6B and S6C).We identified 1,120 and 553 regions (peaks) by ERα-ChIP and FGFR1-ChIP, respectively, that were significantly enriched upon FGF3 treatment. Treatment of CAMA1 cells with each fulvestrant or lucitanib alone or in combination reduced ERα or FGFR1 DNA binding to these new sites (Fig. 5A and B). These results were validated by ChIP-PCR (Supplementary Fig. S6D and S6E). As shown in Fig. 5C and D, ERα and FGFR1 bound to different ERα-related genes, but treatment with lucitanib, fulvestrant, or the combination reduced or abrogated this binding.

To interrogate the functional output of estrogen-independent ERα activity, we classified the genes identified by FGFR1 and ERα ChIP-seq using GSEA. The top enriched gene sets included epithelial mesenchymal transition, *STAT5* signaling, estrogen response early genes, and *p53*-pathways (all FDR < 0.009) after FGFR1 ChIP-seq (Fig. 5E); and estrogen response early genes, estrogen response late genes, *K-Ras* signaling, and *p53*-pathways (all FDR < 0.0001) after ERα ChIP-seq (Fig. 5F). To apply these findings to primary ER^+ breast cancers, we performed RNA-seq analysis on 7 *FGFR1*-amplified and 25 *FGFR1* nonamplified tumors treated with letrozole in the clinical trial. The Volcano plot in Fig. 5G shows that of >24,000 genes analyzed, 280 gene transcripts were increased >2-fold in *FGFR1*-amplified compared with *FGFR1* nonamplified cancers ($P < 0.01$; red dots in Fig. 5G). The top enriched genes by GSEA in *FGFR1*-amplified patients included G_2–M checkpoint genes, *E2F* target genes, estrogen response late genes, and estrogen response early genes (all FDR < 0.01; Fig. 5H; Supplementary Fig. S7). These results further suggest that the ERα pathway is still active in estrogen-deprived (upon letrozole treatment) ER^+/*FGFR1*–amplified primary tumors.

To further elucidate the role of the FGF/FGFR1 axis on ERα signaling, we performed a qRT-PCR profiling assay including 84 ERα regulated genes. FGF3/19 stimulation of estrogen-deprived CAMA1 cells induced >2-fold expression of a subset of ERα target genes, including *TFF1*, *CCND1*, *THSB1*, *CTGF*, *CCL2*, and *EGR3* (Supplementary Fig. S8A). Both FGF3 and FGF19 induced *EGR3*, *CCND1*, and *THSB1* mRNA; this induction was inhibited by treatment with lucitanib, fulvestrant, or the combination (Supplementary Fig. S8B and S8C), and also by transfection of a TK dead K514M FGFR1 mutant into CAMA1 cells (Supplementary Fig. S5D). In line with their higher levels of ERα, FGFR1, and FGF3/4/19 (Figs. 2C and 3D), $CAMA1^{LTED}$ cells expressed higher levels of ERα-regulated genes than CAMA1 parental cells (Supplementary Fig. S8D). Finally, to support our results with lucitanib were not due to off-target effects of the small molecule, we tested the FGFR inhibitor INCB054828 (39). Treatment with INCB054828 also blocked FGF3-induced pFRS2, CAMA1 cell growth, and ERα target gene expression (Supplementary Fig. S9A–S9C).

We next examined the effect of the knockdown of FGFR1 on ERα transcriptional activity. Compared with scrambled control siRNA, knockdown of FGFR1, but not of its major signal transducer FRS2, reduced ERE-luciferase reporter activity (Supplementary Fig. S10A). FGFR1 and FRS2 downregulation was confirmed by immunoblot or RT-PCR, respectively (Supplementary Fig. S10B and S10C). The inability of siFRS2 to reduce ER reporter activity suggested an MEK-independent and PI3K-independent role of the FGFR1 TK on ERα transcriptional function. Supporting this speculation, treatment of CAMA1 cells with lucitanib reduced mRNA levels of the ERα-regulated genes CCND1 and THSB1 more potently than the MEK1/2 inhibitor trametinib (40) and the pan-PI3K inhibitor buparlisib (Supplementary Fig. S10E; ref. 41). In parallel experiments, we confirmed by immunoblot analyses drug-mediated inhibition of their molecular targets: ERα for fulvestrant, pFRS2 and pERK for lucitanib, pERK for trametenib, and pAKT for buparlisib (Supplementary Fig. S10D).

Combined blockade of FGFR1 and ERα potently inhibits growth of ER^+/*FGFR1*–amplified breast cancers

To follow the effect of fulvestrant and lucitanib on ER-dependent gene expression, we next examined whether FGFR1 and/or ERα inhibitors would have an effect on ER^+/*FGFR1*–amplified tumor cell growth. Treatment with the combination of lucitanib and fulvestrant suppressed CAMA1 colony formation in 3D Matrigel significantly more potently than each drug alone (Fig. 6A and B). Western blot analysis of lysates from cells treated for 6 hours showed that only the combination simultaneously reduced levels of pFRS2, pERK1/2, and ERα (Fig. 6C). We next examined the effect of these drugs against two ER^+/$HER2^-$/*FGFR1*–amplified PDXs, T272 and TM00368 (Fig. 6D). Ovariectomized mice with established xenografts ($\geq$250 mm^3) were treated with vehicle, lucitanib, fulvestrant, or both drugs. PDX T272 but not PDXTM00368 required brief estrogen supplementation to generate tumors. In mice bearing PDX T272, the dose of lucitanib was reduced from 10 to 7 mg/kg/day after 3 weeks of therapy due to toxicity in both lucitanib-containing arms. Mice with TM00368 PDXs were treated with 7 mg/kg/day lucitanib. Treatment with the combination of fulvestrant and lucitanib inhibited growth of both PDXs more potently than either drug alone (Fig. 6E; Supplementary Fig. S11A). All mice bearing TM00368 xenografts exhibited a $\geq$50% reduction in tumor size from baseline after 3 weeks of treatment with fulvestrant/lucitanib (Fig. 6F). Biomarkers of response were assessed by IHC in TM00368 tumors harvested at the completion of therapy. Treatment with the combination of lucitanib plus fulvestrant markedly reduced detectable levels of Y653/4 p-FGFR1 and total ERα (Fig. 6G and H). FGFR1 antibody pulldowns of tumor lysates from vehicle- and lucitanib-treated mice coprecipitated ERα. This was not observed in tumors treated with fulvestrant or the combination (Fig. 6I). No change in mouse weight was observed in any of the treatment arms (Supplementary Fig. S11B and S11C).

Discussion

We report herein a novel mechanism by which *FGFR1* amplification confers resistance to antiestrogens in ER^+ breast cancers. In a cohort of postmenopausal patients treated with the aromatase inhibitor letrozole, cancers with *FGFR1* amplification retained tumor cell proliferation, suggesting aberrant FGFR1 signaling is associated with resistance to estrogen deprivation. Short and long-term estrogen deprivation increased total and nuclear FGFR1 and FGF ligand expression in ER^+/*FGFR1*–amplified breast cancer cells and primary tumors. This was associated with an increase in nuclear FGFR1/ERα complexes and maintenance of estrogen-independent transcription of ER-responsive

Published OnlineFirst July 27, 2017; DOI: 10.1158/1078-0432.CCR-17-1232

genes. The interaction between FGFR1 and ERα was blocked by a kinase-dead FGFR1 mutant or by FGFR TKIs. ChIP-seq analysis of FGF-stimulated *FGFR1*-amplified cells showed binding of FGFR1 and of ERα to DNA, which was inhibited by the FGFR TKI lucitanib and by the ER downregulator fulvestrant, respectively, suggesting a possible interdependence between FGFR1 and ERα at transcription start sites. Of note, RNA-seq data from ER$^+$/*FGFR1*–amplified tumors from patients treated with letrozole suggested the ERα pathway is still active (Fig. 5G and H), thus providing a plausible explanation for maintenance of proliferation in these estrogen-deprived cancers. Finally, dual pharmacologic inhibition of FGFR1 and ERα potently inhibited growth of ER$^+$/*FGFR1*–amplified breast cancer cells and PDX models, supporting the clinical development of this combination in patients with this subtype of breast cancer.

FGFR1 in association with nuclear proteins, such as RSK1 and CBP, has been shown to induce gene expression in other cancers (37). As FGFR1 inhibition reduced the transcription of ERα-related genes (Supplementary Fig. S8B and S8C), we speculated the previously reported transcriptional function of FGFR1 (16, 19, 37, 40) may play a role in resistance to estrogen deprivation. Of note, we precipitated both FGFR1 and ERα with C-terminal and N-terminal FGFR1 antibodies from *FGFR1*-amplified CAMA1 cell nuclei (Fig. 4B). These findings were supported by PLA and confocal microscopy studies (Fig. 4C). Inhibition of FGFR1 TK activity with lucitanib and expression of a TK dead K514M FGFR1 mutant into CAMA1 cells reduced ERα-dependent gene transcription (Supplementary Fig. S8B and S8C; Supplementary Fig. S5D) and inhibited the association of FGFR1 with ERα (Fig. 4E–H). Taken together, these data support a novel TK-dependent role of nuclear FGFR1 on ERα-dependent gene transcription in estrogen-independent ER$^+$/*FGFR1*-amplified breast cancers.

To the best of our knowledge, this is the first report of a physical association of FGFR1 and ERα associated with antiestrogen resistance. It follows studies supporting both the nuclear localization and function of FGFR1. FGFR1 can enter the nucleus by retrograde transport from the endoplasmic reticulum lumen to the cytosol via Sec61p channels before endoplasmic vesicles deliver the receptor to the plasma membrane (17, 41). This process is possible because of the atypical TMD of FGFR1, which consists of nonpolar amino acid chains interrupted by polar regions in a β-sheet structure, thus allowing mobilization of the receptor out of the membrane (17, 41). Cell surface biotinylation assays show that nuclear FGFR1 can also originate from the cell surface (42), suggesting FGFR1 is internalized and traffics to the nucleus via endosomal pathways. Indeed, FGFR1 and FGFR2 can translocate to the nucleus following ligand stimulation in pancreatic stellate cells; this process requires the interaction of FGFR1 with nuclear import proteins, like importin β (15, 43). Once in the nucleus, FGFR1 has been shown to regulate gene transcription (16, 19, 37, 40). Nuclear targeting of FGFR1 by substituting its signal peptide for a nuclear localization sequence is sufficient to initiate DNA synthesis and transcription of c-Jun, an activator of cyclin D1. Removal of the kinase region of nuclear-targeted FGFR1 ablates this effect (44). These data suggest the TK function of FGFR1 is necessary for its transcriptional role, consistent with our data from ER$^+$/*FGFR1*–amplified breast cancer cells shown herein.

In summary, we have identified a mechanism by which amplified *FGFR1* can sustain estrogen-independent breast tumor growth. We propose this mechanism explains, in part, the limited effects of estrogen deprivation on ER$^+$/*FGFR1*–amplified breast cancers in the clinical trial with letrozole. On the basis of these data, we propose combinations of ERα and FGFR antagonists should be tested in patients with ER$^+$/*FGFR1*–amplified breast cancer.

Disclosure of Potential Conflicts of Interest

J.M. Giltnane is an employee of Genentech. I.A. Mayer reports receiving commercial research grants from Genentech and Pfizer and is a consultant/advisory board member for AstraZeneca and Novartis. C.L. Arteaga is a member of an advisory board for Novartis. No potential conflicts of interest were disclosed by the other authors.

Authors' Contributions

Conception and design: L. Formisano, Y. Lu, J.M. Balko, O. Deas, T. Stricker, C.L. Arteaga

Development of methodology: L. Formisano, K.M. Stauffer, C.D. Young, Y. Lu, J.M. Balko, M. Sanders, C.L. Arteaga

Acquisition of data (provided animals, acquired and managed patients, provided facilities, etc.): L. Formisano, K.M. Stauffer, C.D. Young, V.M. Jansen, M.M. Estrada, K.E. Hutchinson, J.M. Giltnane, J.M. Balko, O. Deas, S. Cairo, J.-G. Judde, I.A. Mayer, M. Sanders, T.C. Dugger, C.L. Arteaga

Analysis and interpretation of data (e.g., statistical analysis, biostatistics, computational analysis): L. Formisano, K.M. Stauffer, C.D. Young, N.E. Bhola, A.L. Guerrero-Zotano, V.M. Jansen, K.E. Hutchinson, J.M. Giltnane, Y. Lu, J.M. Balko, O. Deas, S. Cairo, I.A. Mayer, M. Sanders, T. Stricker, C.L. Arteaga

Writing, review, and/or revision of the manuscript: L. Formisano, K.M. Stauffer, C.D. Young, N.E. Bhola, A.L. Guerrero-Zotano, V.M. Jansen, K.E. Hutchinson, L.J. Schwarz, Y. Lu, J.M. Balko, I.A. Mayer, M. Sanders, R. Bianco, T. Stricker, C.L. Arteaga

Administrative, technical, or material support (i.e., reporting or organizing data, constructing databases): L. Formisano, A.L. Guerrero-Zotano, M.M. Estrada, J.M. Giltnane, T.C. Dugger, C.L. Arteaga

Study supervision: J.-G. Judde, R. Bianco, C.L. Arteaga

Acknowledgments

The authors thank Drs. Scott Hiebert and Charles Sanders for helpful discussions and review of this manuscript.

Grant Support

This study was funded by NIH Breast SPORE grant P50 CA098131, Vanderbilt-Ingram Cancer Center Support grant P30 CA68485, Susan G. Komen for the Cure Foundation grant SAC100013 (to C.L. Arteaga), and a grant from the Breast Cancer Research Foundation (to C.L. Arteaga). J.M. Balko was supported by NIH/NCI4R00 CA181491 grant and Susan G. Komen Career Catalyst Research award CCR 299052. V.M. Jansen was supported by Conquer Cancer Foundation ASCO Young Investigator Award 8364 and Susan G. Komen Postdoctoral Fellowship Grant PDF15329319. T.P. Stricker was supported by NIH grant K08 CA148912.

The costs of publication of this article were defrayed in part by the payment of page charges. This article must therefore be hereby marked *advertisement* in accordance with 18 U.S.C. Section 1734 solely to indicate this fact.

Received April 27, 2017; revised June 12, 2017; accepted July 19, 2017; published OnlineFirst July 27, 2017.

References

1. Courjal F, Cuny M, Simony-Lafontaine J, Louason G, Speiser P, Zeillinger R, et al. Mapping of DNA amplifications at 15 chromosomal localizations in 1875 breast tumors: definition of phenotypic groups. Cancer Res 1997;57:4360–7.

2. Jacquemier J, Adelaide J, Parc P, Penault-Llorca F, Planche J, deLapeyriere O, et al. Expression of the FGFR1 gene in human breast-carcinoma cells. Int J Cancer 1994;59:373–8.
3. Reis-Filho JS, Simpson PT, Turner NC, Lambros MB, Jones C, Mackay A, et al. FGFR1 emerges as a potential therapeutic target for lobular breast carcinomas. Clin Cancer Res 2006;12:6652–62.
4. Gorringe KL, Jacobs S, Thompson ER, Sridhar A, Qiu W, Choong DY, et al. High-resolution single nucleotide polymorphism array analysis of epithelial ovarian cancer reveals numerous microdeletions and amplifications. Clin Cancer Res 2007;13:4731–9.
5. Simon R, Richter J, Wagner U, Fijan A, Bruderer J, Schmid U, et al. High-throughput tissue microarray analysis of 3p25 (RAF1) and 8p12 (FGFR1) copy number alterations in urinary bladder cancer. Cancer Res 2001; 61:4514–9.
6. Missiaglia E, Selfe J, Hamdi M, Williamson D, Schaaf G, Fang C, et al. Genomic imbalances in rhabdomyosarcoma cell lines affect expression of genes frequently altered in primary tumors: an approach to identify candidate genes involved in tumor development. Genes Chromosomes Cancer 2009;48:455–67.
7. Jiang T, Gao G, Fan G, Li M, Zhou C. FGFR1 amplification in lung squamous cell carcinoma: a systematic review with meta-analysis. Lung Cancer 2015;87:1–7.
8. Turner N, Pearson A, Sharpe R, Lambros M, Geyer F, Lopez-Garcia MA, et al. FGFR1 amplification drives endocrine therapy resistance and is a therapeutic target in breast cancer. Cancer Res 2010;70:2085–94.
9. Schlessinger J, Plotnikov AN, Ibrahimi OA, Eliseenkova AV, Yeh BK, Yayon A, et al. Crystal structure of a ternary FGF-FGFR-heparin complex reveals a dual role for heparin in FGFR binding and dimerization. Mol Cell 2000;6:743–50.
10. Turner N, Grose R. Fibroblast growth factor signalling: from development to cancer. Nat Rev Cancer 2010;10:116–29.
11. Bryant DM, Stow JL. Nuclear translocation of cell-surface receptors: lessons from fibroblast growth factor. Traffic 2005;6:947–54.
12. Zammit C, Barnard R, Gomm J, Coope R, Shousha S, Coombes C, et al. Altered intracellular localization of fibroblast growth factor receptor 3 in human breast cancer. J Pathol 2001;194:27–34.
13. Cerliani JP, Guillardoy T, Giulianelli S, Vaque JP, Gutkind JS, Vanzulli SI, et al. Interaction between FGFR-2, STAT5, and progesterone receptors in breast cancer. Cancer Res 2011;71:3720–31.
14. Stachowiak MK, Birkaya B, Aletta JM, Narla ST, Benson CA, Decker B, et al. "Nuclear FGF receptor-1 and CREB binding protein: an integrative signaling module". J Cell Physiol 2015;230:989–1002.
15. Coleman SJ, Chioni AM, Ghallab M, Anderson RK, Lemoine NR, Kocher HM, et al. Nuclear translocation of FGFR1 and FGF2 in pancreatic stellate cells facilitates pancreatic cancer cell invasion. EMBO Mol Med 2014;6:467–81.
16. Chioni AM, Grose R. FGFR1 cleavage and nuclear translocation regulates breast cancer cell behavior. J Cell Biol 2012;197:801–17.
17. Myers JM, Martins GG, Ostrowski J, Stachowiak MK. Nuclear trafficking of FGFR1: a role for the transmembrane domain. J Cell Biochem 2003; 88:1273–91.
18. Stachowiak MK, Fang X, Myers JM, Dunham SM, Berezney R, Maher PA, et al. Integrative nuclear FGFR1 signaling (INFS) as a part of a universal "feed-forward-and-gate" signaling module that controls cell growth and differentiation. J Cell Biochem 2003;90:662–91.
19. Terranova C, Narla ST, Lee YW, Bard J, Parikh A, Stachowiak EK, et al. Global developmental gene programing involves a nuclear form of fibroblast growth factor receptor-1 (FGFR1). PLoS One 2015;10:e0123380.
20. Katoh M. WNT and FGF gene clusters (review). Int J Oncol 2002;21: 1269–73.
21. Brady N, Chuntova P, Bade LK, Schwertfeger KL. The FGF/FGFR axis as a therapeutic target in breast cancer. Expert Rev Endocrinol Metab 2013;8:391–402.
22. Cuny M, Kramar A, Courjal F, Johannsdottir V, Iacopetta B, Fontaine H, et al. Relating genotype and phenotype in breast cancer: an analysis of the prognostic significance of amplification at eight different genes or loci and of p53 mutations. Cancer Res 2000;60:1077–83.
23. Balko JM, Mayer IA, Sanders ME, Miller TW, Kuba MG, Meszoely IM, et al. Discordant cellular response to presurgical letrozole in bilateral synchronous ER+ breast cancers with a KRAS mutation or FGFR1 gene amplification. Mol Cancer Ther 2012;11:2301–5.
24. Allred DC, Harvey JM, Berardo M, Clark GM. Prognostic and predictive factors in breast cancer by immunohistochemical analysis. Mod Pathol 1998;11:155–68.
25. Miller TW, Balko JM, Fox EM, Ghazoui Z, Dunbier A, Anderson H, et al. ER alpha-dependent E2F transcription can mediate resistance to estrogen deprivation in human breast cancer. Cancer Discov 2011;1:338–51.
26. Bhola NE, Jansen VM, Bafna S, Giltnane JM, Balko JM, Estrada MV, et al. Kinome-wide functional screen identifies role of PLK1 in hormone-independent, ER-positive breast cancer. Cancer Res 2015;75:405–14.
27. Kim D, Pertea G, Trapnell C, Pimentel H, Kelley R, Salzberg SL. TopHat2: accurate alignment of transcriptomes in the presence of insertions, deletions and gene fusions. Genome Biol 2013;14:R36.
28. DeLuca DS, Levin JZ, Sivachenko A, Fennell T, Nazaire MD, Williams C, et al. RNA-SeQC: RNA-seq metrics for quality control and process optimization. Bioinformatics 2012;28:1530–2.
29. Dowsett M, Smith IE, Ebbs SR, Dixon JM, Skene A, A'Hern R, et al. Prognostic value of Ki67 expression after short-term presurgical endocrine therapy for primary breast cancer. J Natl Cancer Inst 2007;99: 167–70.
30. Dixon JM, Renshaw L, Young O, Murray J, Macaskill EJ, McHugh M, et al. Letrozole suppresses plasma estradiol and estrone sulphate more completely than anastrozole in postmenopausal women with breast cancer. J Clin Oncol 2008;26:1671–6.
31. Wolff B, Sanglier JJ, Wang Y. Leptomycin B is an inhibitor of nuclear export: Inhibition of nucleo-cytoplasmic translocation of the human immunodeficiency virus type 1 (HIV-1) Rev protein and Rev-dependent mRNA. Chem Biol 1997;4:139–47.
32. Kwek SS, Roy R, Zhou H, Climent J, Martinez-Climent JA, Fridlyand J, et al. Co-amplified genes at 8p12 and 11q13 in breast tumors cooperate with two major pathways in oncogenesis. Oncogene 2009;28:1892–903.
33. Gao J, Aksoy BA, Dogrusoz U, Dresdner G, Gross B, Sumer SO, et al. Integrative analysis of complex cancer genomics and clinical profiles using the cBioPortal. Sci Signal 2013;6:pl1.
34. Cerami E, Gao J, Dogrusoz U, Gross BE, Sumer SO, Aksoy BA, et al. The cBio cancer genomics portal: an open platform for exploring multidimensional cancer genomics data. Cancer Discov 2012;2:401–4.
35. Gyorffy B, Lanczky A, Eklund AC, Denkert C, Budczies J, Li Q, et al. An online survival analysis tool to rapidly assess the effect of 22,277 genes on breast cancer prognosis using microarray data of 1,809 patients. Breast Cancer Res Treat 2010;123:725–31.
36. Bello E, Colella G, Scarlato V, Oliva P, Berndt A, Valbusa G, et al. E-3810 is a potent dual inhibitor of VEGFR and FGFR that exerts antitumor activity in multiple preclinical models. Cancer Res 2011;71:1396–405.
37. Dunham-Ems SM, Lee YW, Stachowiak EK, Pudavar H, Claus P, Prasad PN, et al. Fibroblast growth factor receptor-1 (FGFR1) nuclear dynamics reveal a novel mechanism in transcription control. Mol Biol Cell 2009;20: 2401–12.
38. Sosa LD, Gutierrez S, Petiti JP, Vaca AM, De Paul AL,Torres AI. Cooperative effect of E-2 and FGF2 on lactotroph proliferation triggered by signaling initiated at the plasma membrane. Am J Physiol-Endoc M 2013;305: E41–E9.
39. Liu PCC, Wu LX, Koblish H, Bowman K, Zhang Y, Klabe R, et al. Preclinical characterization of the selective FGFR inhibitor INCB054828. Cancer Res In: Proceedings of the 106th Annual Meeting of the American Association for Cancer Research; 2015 Apr 18–22; Philadelphia, PA. Philadelphia, PA: AACR; 2015. Abstract nr 771.
40. Somanathan S, Stachowiak EK, Siegel AJ, Stachowiak MK, Berezney R. Nuclear matrix bound fibroblast growth factor receptor is associated with splicing factor rich and transcriptionally active nuclear speckles. J Cell Biochem 2003;90:856–69.
41. Romisch K. Surfing the Sec61 channel: bidirectional protein translocation across the ER membrane. J Cell Sci 1999;112(Pt 23):4185–91.
42. Bryant DM, Wylie FG, Stow JL. Regulation of endocytosis, nuclear translocation, and signaling of fibroblast growth factor receptor 1 by E-cadherin. Mol Biol Cell 2005;16:14–23.
43. Reilly JF, Maher PA. Importin beta-mediated nuclear import of fibroblast growth factor receptor: role in cell proliferation. J Cell Biol 2001;152: 1307–12.
44. Wiedlocha A, Falnes PO, Madshus IH, Sandvig K, Olsnes S. Dual mode of signal transduction by externally added acidic fibroblast growth factor. Cell 1994;76:1039–51.

Clinical Cancer Research

Correction: Association of FGFR1 with ERα Maintains Ligand-Independent ER Transcription and Mediates Resistance to Estrogen Deprivation in ER$^+$ Breast Cancer

Luigi Formisano, Kimberly M. Stauffer, Christian D. Young, Neil E. Bhola, Angel L. Guerrero-Zotano, Valerie M. Jansen, Mónica M. Estrada, Katherine E. Hutchinson, Jennifer M. Giltnane, Luis J. Schwarz, Yao Lu, Justin M. Balko, Olivier Deas, Stefano Cairo, Jean-Gabriel Judde, Ingrid A. Mayer, Melinda Sanders, Teresa C. Dugger, Roberto Bianco, Thomas Stricker, and Carlos L. Arteaga

In the original version of this article (1), the stated disclosure of the author Carlos L. Arteaga is incorrect. The error has been corrected in the latest online HTML and PDF versions of the article. The authors regret this error.

Reference

1. Formisano L, Stauffer KM, Young CD, Bhola NE, Guerrero-Zotano AL, Jansen VM. Association of FGFR1 with ERα maintains ligand-independent ER transcription and mediates resistance to estrogen deprivation in ER$^+$ breast cancer. Clin Cancer Res 2017;23:6138–50.

Published first February 15, 2019.
doi: 10.1158/1078-0432.CCR-18-4268

Published OnlineFirst July 27, 2017; DOI: 10.1158/1078-0432.CCR-17-1232

AACR American Association for Cancer Research

Clinical Cancer Research

Association of FGFR1 with ERα Maintains Ligand-Independent ER Transcription and Mediates Resistance to Estrogen Deprivation in ER$^+$ Breast Cancer

Luigi Formisano, Kimberly M. Stauffer, Christian D. Young, et al.

Clin Cancer Res 2017;23:6138-6150. Published OnlineFirst July 27, 2017.